Proceedings of the 21st ICSMGE, Vienna, Austria, 14 – 19 June 2026. Pistrol, Adam & Schweiger (eds.)
Published by: ÖGG, Austrian Society for Geomechanics, Salzburg, Austria, ISBN 978-3-9503898-4-5
https://doi.org/10.53243/ICSMGE2026-591

Effect of Drainage System on the Stability of CAES Cavern

Aohui Zhou, Wenbin Fei
College of Civil Engineering, Hunan University, Changsha, Hunan,410082, China

Peng Li
Powerchina Zhongnan Engineering co., LTD., Changsha, Hunan,410014, China

ABSTRACT: With the large-scale integration of renewable energy sources like wind and solar, the demand for energy storage has surged. Currently, only pumped hydro storage and salt cavern compressed air energy storage (CAES) operate commercially on a large scale. However, lined rock cavern (LRC) gas storage, free from many limitations, is gaining attention. While prior studies focus on LRC sealing and stability, the role of drainage systems—a critical component—has been overlooked. Structurally, drainage systems can introduce defects in LRC linings, but their impact on stability remains unstudied. This study examines the effects of drainage system parameters (pipe spacing: 1m, 2m; pipe diameter: 10cm, 15cm) and lateral pressure coefficients (0.8, 1.0, 1.2) using numerical simulations during LRC excavation and operation phases. Stress and deformation in the steel lining, concrete, and surrounding rock are analyzed. Results show minimal drainage impact during excavation, with only localized stress in C25 concrete. However, during operation, increasing pipe diameter and reducing spacing significantly worsen surrounding rock deformation, concrete damage, and steel lining stress and fatigue. Pipe diameter has a stronger effect than spacing. Under the most adverse conditions (spacing: 1m; diameter: 15cm; pressure coefficient: 0.8), roof and side displacements increase by 1.45mm and 0.42mm, steel lining stress rises by 29.89MPa, and fatigue amplitude grows by 10.85MPa. Stability is best at a pressure coefficient of 1.0 or 1.2 and poorest at 0.8. These findings highlight that while drainage systems may be negligible in conventional tunnel designs, they are crucial for LRC under cyclic high pressures, necessitating optimized design parameters.

KEYWORDS: Compressed air energy storage, Lined rock caverns, Drainage System, Stability analysis, In-situ Stresses

1 INTRODUCTION

In response to the escalating crises of non-renewable energy depletion and environmental degradation, China unveiled its Dual Carbon Strategy in 2020. To advance this national agenda, recent years have witnessed a concerted push toward the rapid development of renewable energy industries. In 2024, China's total wind and solar installed power generation capacity had reached approximately 0.52 and 0.89 billion kilowatts in 2024, representing a year-on-year increase of 18.0% and 45.2 (National-Energy-Administration, 2025). Despite these advances, the inherently intermittent, stochastic, and fluctuating nature of wind and solar resources presents significant challenges. Consequently, to facilitate greater integration of renewable energy into the grid, the deployment of energy storage systems has become imperative. These systems are essential to mitigating the adverse impacts of renewable intermittency on grid reliability and operational security (Liang et al., 2024).

In this context, large-scale compressed air energy storage (CAES) have rapidly become an engineering hotspot. The lined rock cavern (LRC), due to its extremely low dependence on geological conditions, has become the ideal gas storage medium for CAES (Jiang et al., 2020). A typical LRC structural configuration is illustrated in Figure 1. From the interior to the exterior, the cavern typically comprises a sealing layer, a concrete lining, a drainage system, a shotcrete layer, and the surrounding rock. Under idealized conditions, the sealing layer serves to retain high-pressure gas, while the surrounding rock bears the majority of the loads induced by the internal pressure. The concrete lining primarily functions as a medium for load transfer. The drainage system serves to alleviate excessive external hydro pressure during low-pressure storage and maintenance periods, thereby preventing reverse buckling deformation of the thin sealing layer or the formation of substantial gaps between the sealing layer and the concrete lining. However, the drainage pipes located behind the concrete lining are analogous to voids commonly observed behind linings in conventional tunnel engineering. These elements may be regarded as inherent defects within the lining structure and pose a potential threat to the overall stability of the LRC under high internal pressure. Despite this, most existing studies simplify the drainage system, routinely neglecting the influence of the drainage system on structural performance.

To investigate the influence of the drainage system on LRC, this study develops a numerical model incorporating drainage system across excavation and operation stages. The model evaluates the coupled effects of drainage system and lateral pressure coefficients on the stress distribution and deformation behaviour of the LRC, thereby elucidating their roles in governing overall structural performance.

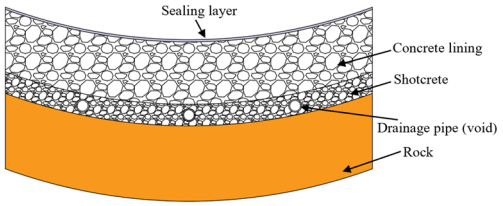

Figure 1. Typical lined rock cavern structural configuration.

2 NUMERICAL MODEL

2.1 *Model Establishment*

Numerical simulations were conducted using ABAQUS. The global model geometry, shown in Fig. 2(a), spans 200 m × 150 m, with a cavern radius of 5 m and burial depth of 100 m. The structural composition of the LRC, from the interior to outward, comprises (Fig. 2(b)): (1) 20 mm steel lining (Q345R); (2) 580 mm concrete lining (C30); (3) 200 mm shotcrete (C25); (4) drainage pipes (PVC); and (5) the surrounding rock. Material properties and constitutive models are listed in Table 1.

The model assumptions are as following: (1) Since the length-to-diameter ratio of cavern exceeds 250, the model is idealized as a two-dimensional plane strain problem; (2) Both x- and y- displacements are fixed at the bottom, while two sides are restricted in the x-displacement; (3) The interfaces between C25 and surrounding rock, as well as between C25 and C30 are modelled as common nodes. Frictional interfaces are defined

between C25 and drainage pipes, as well as between steel lining and C30.

The model is computed through the following sequence: (1) In-situ stress initialization; (2) Excavation process adopts a stress reduction method to simulate the support effect of the lining, with stress released in three stages (65%, 90%, and 100%) corresponding to different phases; (3) Compressed air is applied as cyclic internal pressure, varying from 4 MPa to 10 MPa during charging and discharging (Fig. 2(c)).

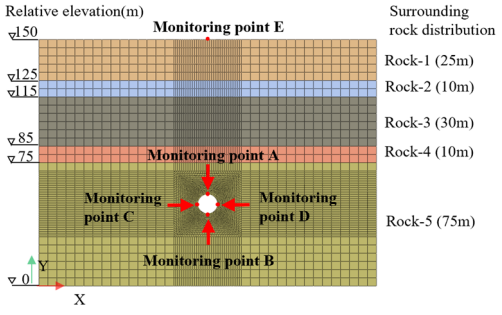

(a) Overall Model

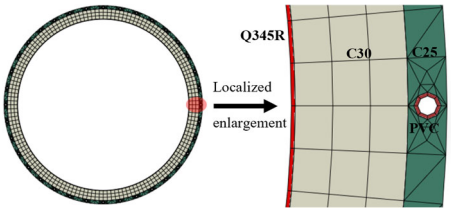

(b) Steel lining- concrete lining- shotcrete-drainage pipes

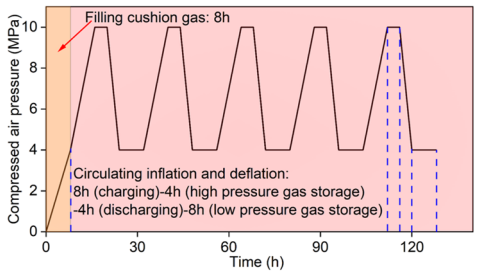

(c) Cyclic air pressure

Figure 2. Simulation model

Table 1. Model parameters

Materials	Constitutive	Density (kg/m3)	Elastic modulus (GPa)	Poisson's ratio
Q345R	Plasticity	7850	206	0.3
C30	CDP	2400	30	0.2
C25	CDP	2400	28	0.2
PVC	Elastic	1400	3	0.4
Rock-1	M-C	2100	2.5	0.37
Rock-2	M-C	2200	4	0.35
Rock-3	M-C	2550	6	0.32
Rock-4	M-C	2650	8	0.28
Rock-5	M-C	2700	12	0.27

Note: CDP = Concrete Damage Plasticity; M-C = Mohr-Coulomb; Rock-1 = Strongly weathered basalt; Rock-2 = Strongly weathered basalt; Rock-3 = Moderately weathered basalt; Rock-4 = Slightly weathered basalt; Rock-5 = Slightly weathered basalt

2.2 *Simulation scenarios*

To evaluate the effects of different design parameters, fifteen simulation scenarios were established by varying three key factors, as shown in Fig. 3: drainage pipe spacing S (1 m, 2 m), pipe diameter D (10 cm, 15 cm), and lateral pressure coefficient λ (A: 0.8; B: 1.0; C: 1.2). The scenario number is λ-S-D. For example, A-1-15 represents λ = 0.8, S = 1m, D = 15cm.

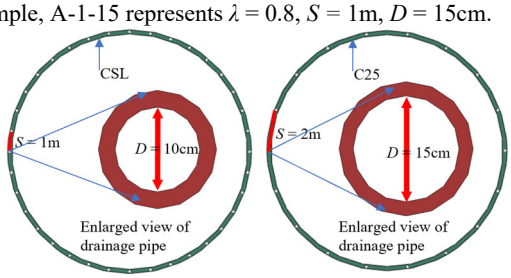

Figure 3. Drainage pipes layout.

3 STRUCTURAL RESPONSE AFTER EXCAVATION

3.1 *Surrounding rock*

After excavation, the horizontal displacement pattern is symmetric, with inward contraction on both sides of the cavern while vertical displacement reveals settlement at the roof and uplift at the floor. As the lateral pressure coefficient increases, horizontal deformation intensifies, whereas vertical movements attenuate. The plastic strain zone (It is characterized by the equivalent plastic strain PEEQ, which represents the cumulative plastic strain of the surrounding rock) initially concentrated at the sidewalls gradually migrates toward the roof and floor, though plastic deformation remains limited, with hydrostatic loading yielding the lowest values. Quantitative analysis from monitoring points (Table 2) shows that the displacement difference between cases with and without drainage are all less than 0.03 mm, indicates that drainage configuration exerts a negligible influence on surrounding rock displacement during excavation.

Table 2. Displacement of rock monitoring points after excavation

Scenario No.	A: Roof (mm)	B: Floor (mm)	C: Left side (mm)	D: Right side (mm)	E: Ground (mm)
A-0-0	-1.60	+1.52	+0.98	-0.98	-0.27
A-1-10	-1.61	+1.52	+0.98	-0.98	-0.27
A-1-15	-1.61	+1.53	+0.98	-0.98	-0.27
A-2-10	-1.60	+1.52	+0.98	-0.98	-0.27
A-2-15	-1.61	+1.53	+0.98	-0.98	-0.27
B-0-0	-1.45	+1.39	+1.40	-1.40	-0.25
B-1-10	-1.48	+1.40	+1.42	-1.42	-0.25
B-1-15	-1.47	+1.40	+1.41	-1.41	-0.25
B-2-10	-1.46	+1.40	+1.40	-1.40	-0.25
B-2-15	-1.46	+1.40	+1.40	-1.40	-0.25
C-0-0	-1.30	+1.27	+1.82	-1.82	-0.22
C-1-10	-1.31	+1.27	+1.82	-1.82	-0.22
C-1-15	-1.31	+1.27	+1.83	-1.83	-0.23
C-2-10	-1.31	+1.27	+1.82	-1.82	-0.22
C-2-15	-1.31	+1.28	+1.82	-1.82	-0.23

3.2 *Concrete and steel*

Stress in concrete layers demonstrates a more pronounced response (Table 3). C25 subjected to secondary and tertiary stress release stages, exhibits marked stress concentrations

around drainage pipelines—particularly with increasing pipe diameter. For instance, the maximum compressive stress in C25 escalates from 2.41 MPa (A-0-0) to 7.61 MPa (A-1-15), and further to 8.17 MPa with increased spacing (A-2-15). In contrast, C30 only experiences the final stress release stage, undergoing much lower stress levels, with limited sensitivity to drainage pipes. The lateral pressure coefficient influences the maximum stress. When $\lambda = 1$, the stress on the concrete is at its lowest.

Table 3. Stress in concrete after excavation

Scenario No.	C25 (MPa)	C30 (MPa)
A-0-0	2.41	0.65
A-1-10	4.94	0.65
A-1-15	7.61	0.73
A-2-10	5.10	0.65
A-2-15	8.17	0.76
B-0-0	2.32	0.61
B-1-10	4.83	0.65
B-1-15	7.38	0.72
B-2-10	4.95	0.61
B-2-15	7.98	0.76
C-0-0	2.92	0.78
C-1-10	5.95	0.79
C-1-15	8.63	0.99
C-2-10	6.21	0.79
C-2-15	9.59	1.04

The steel lining only bears the load from the final stress release, showing uniformly low von Mises stress levels. Neither the presence nor the layout of drainage pipes significantly affects the steel lining's stress response, although stress magnitudes increase with the lateral pressure coefficient.

In summary, the influence of the drainage system on the excavation stage is negligible.

4 STRUCTURAL RESPONSE DURING OPERATION

4.1 *Surrounding rock*

The deformation performance during the operation of the surrounding rock is presented in Fig.4. The internal pressure applied cyclically loads the surrounding rock, resulting in distinct displacement patterns: the roof shifts from settlement to uplift, the floor from uplift to settlement, and the sidewalls transition from inward convergence to outward expansion. These deformations are accompanied by a progressive increase in plastic strain. The monitoring data reveal the following key trends: (1) Roof uplift is the most pronounced among all monitored locations, followed by sidewall expansion, while floor settlement remains relatively small. Ground surface displacement consistently remains around 1 mm across all cases. (2) Introducing a drainage system increases overall deformation, particularly when the pipe radius $D = 15$ cm. (3) As λ increases from 0.8 to 1.2, displacements at the roof, floor, and sides progressively decrease, while surface uplift experiences a marginal increase. This suggests that a greater lateral pressure coefficient helps suppress cavern deformation. Plastic zone after five operational cycles shows a geometric evolution from a vertically elongated ellipse ($\lambda = 0.8$) to a more circular form ($\lambda = 1.0$), and eventually a horizontally elongated shape ($\lambda = 1.2$). With drainage pipes, although the overall extent of the plastic zone remains similar, localized plastic strain concentrations appear intermittently around the cavern periphery—particularly intensified for larger pipe diameters. This implies that drainage systems may exacerbate localized instability, potentially triggering preferential zones of failure.

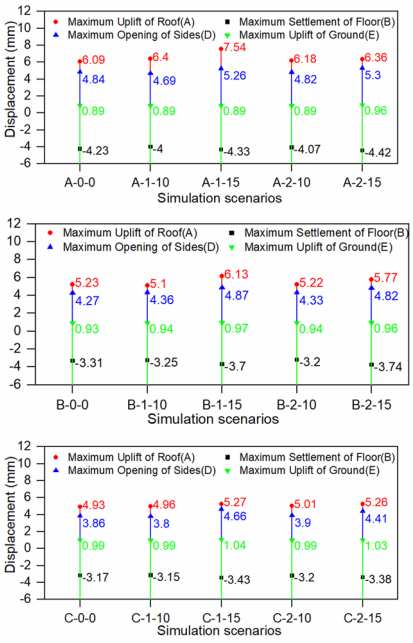

(a) Maximum displacement of the surrounding rock

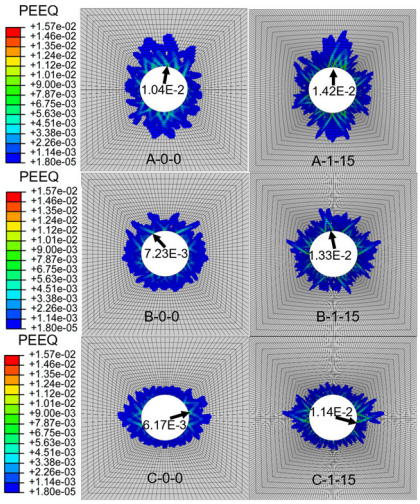

(b) Plastic strain zone

Figure 4. Surrounding rock deformation property during operation.

4.2 *Concrete*

The minimum principal stress and damage distribution in the concrete (C25 and C30) at the end of the fifth cycle are illustrated in Fig.5. Under operational loading, C30 bears higher compressive stress compared to C25. In caverns without drainage, the load is distributed uniformly across the concrete layers, with maximum stress within 10 MPa. However, when a drainage system is present, stress transfer becomes uneven. Internal pressures tend to concentrate around the drainage pipe interfaces, producing localized stress peaks—particularly in C25 and extending into the adjacent C30. The drainage pipe diameter plays a decisive role in the stress pattern. When $D =$ 10 cm, the greater thickness of the C25 leads to a dominant share of the compressive stress being borne by this layer, with the C30 experiencing nearly half the stress level (A-1-10 C25: 19.47MPa; A-1-10 C30: 10.49MPa). Conversely, when $D = 15$ cm, the reduced thickness of C25 shifts a greater portion of the load to the C30, resulting in comparable or even higher stress

in the C30 lining (A-1-15 C25: 15.00MPa; A-1-15 C30: 15.52MPa). Operational loading also results in significantly greater stress magnitudes and damage compared to the excavation stage. Caverns with drainage systems exhibit more severe and spatially extensive damage, especially along pipe alignments.

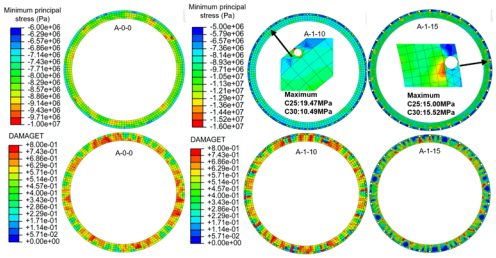

Figure 5. Concrete stress and damage during operation.

In conclusion, the drainage pipes induce localized stress concentrations and amplify structural damage.

4.3 *Steel*

The presence of a drainage system increases both the maximum Mises stress and its cyclic variation in the steel lining during operation (Fig.6). For instance, under 10 MPa air pressure, the maximum Mises stress increases from 300.24 MPa (A-0-0) to 330.13 MPa (A-1-15), representing a rise of 29.89 MPa. The stress difference increases from 110.09 MPa (A-0-0) to 120.94 MPa (A-1-15) between low- and high-cycle loading. Across all cases, hydrostatic pressure yields the lowest stress levels, while $\lambda = 0.8$ produces the highest. Given CAES systems are designed for over 20,000 cycles, this rise in mean stress and amplitude notably reduces fatigue life. These findings suggest that drainage systems, particularly with larger diameters, may compromise long-term durability of the steel sealing layer.

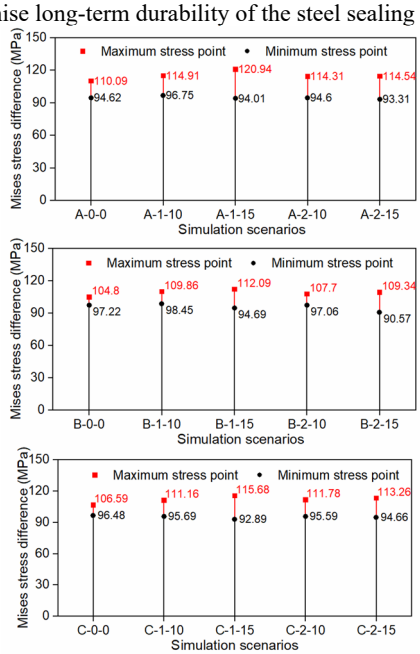

Figure 6. Mises stress difference of steel lining during operation.

5 DISCUSSION

Table 4 summarizes the mechanical response of the LRC. During the operation, the roof changes from settlement to uplift, the floor from uplift to settlement, and the sidewalls shift from inward contraction to outward expansion. Among these, the roof exhibits the largest displacement variation, followed by the sides and the floor, with ground surface movement remaining minimal. Upon entering the operational phase, steel lining stress increases substantially. When $D = 15$ cm, displacements at monitoring points rise relative to the no-drainage scenario. In contrast, $D = 10$ cm leads to slight reductions in some locations, though all are within 0.23 mm. Overall, the installation of drainage enhances surrounding rock deformation and elevates peak stress in the steel lining, with pipe diameter having a more significant influence than spacing. Meanwhile, increasing the lateral pressure coefficient reduces the difference in deformation between excavation and operation. The displacement change under hydrostatic loading is similar to that at $\lambda = 1.2$. The lowest stress in steel when $\lambda = 1.0$, followed by $\lambda = 1.2$, and peak significantly at $\lambda = 0.8$. These trends indicate that the structural stability of the LRC is most favorable at $\lambda = 1.0$ and 1.2, while $\lambda = 0.8$ represents the least stable condition.

Table 4. Differences in deformation of rock between excavation and operation stages and maximum steel lining stress during operation

Scenario No.	Surrounding rock				Steel lining
	Roof (mm)	Floor (mm)	Sides (mm)	Ground (mm)	Maximum Stress (MPa)
A-0-0	7.69	-5.75	5.82	1.16	300.24
A-1-10	8.01	-5.52	5.67	1.16	308.55
A-1-15	9.15	-5.86	6.24	1.16	330.13
A-2-10	7.78	-5.59	5.8	1.16	307.47
A-2-15	7.97	-5.95	6.28	1.23	313.30
B-0-0	6.68	-4.7	5.67	1.18	256.49
B-1-10	6.58	-4.65	5.78	1.19	264.88
B-1-15	7.6	-5.10	6.28	1.22	283.04
B-2-10	6.68	-4.60	5.73	1.19	260.26
B-2-15	7.23	-5.14	6.22	1.21	277.82
C-0-0	6.23	-4.44	5.68	1.21	259.17
C-1-10	6.27	-4.42	5.62	1.21	264.86
C-1-15	6.58	-4.7	6.49	1.27	286.14
C-2-10	6.32	-4.47	5.72	1.21	267.32
C-2-15	6.57	-4.66	6.23	1.26	284.32

6 CONCLUSION

(1) In the excavation phase, the drainage system mainly influences stress in the C25, with minimal impact on stability.
(2) In the operation phase, cyclic high pressure causes significant stress concentration and concrete failure in models with drainage systems, leading to greater surrounding rock deformation and increased stress and fatigue on the steel lining.
(3) Lateral pressure coefficient affects both deformation and steel lining stress; the best stability is observed at $\lambda = 1.2$ and under hydrostatic pressure, while $\lambda = 0.8$ is least favorable.
(4) Due to increased deformation and stress under cyclic loading, drainage systems affect LRC performance during operation and must be considered in CAES design.

7 REFERENCES

JIANG, Z., LI, P., TANG, D., ZHAO, H. & LI, Y. 2020. Experimental and Numerical Investigations of Small-Scale Lined Rock Cavern at Shallow Depth for Compressed Air Energy Storage. Rock Mechanics and Rock Engineering, 53, 2671-2683.

LIANG, Y., LI, P., XING, L., SU, W., LI, W. & XU, W. 2024. Current status of thermodynamic electricity storage: Principle, structure, storage device and demonstration. Journal of Energy Storage, 80.

NATIONAL-ENERGY-ADMINISTRATION. 2025. The National Energy Administration released statistics on the national power industry in 2024 [Online].